

1 Manuscript of the article:
2 Gelybó, Gy., Barcza, Z., Kern, A., Kljun, N., 2013. Effect of spatial heterogeneity on
3 the validation of remote sensing based GPP estimations. *Agricultural and Forest
4 Meteorology*, 174-175, 43-53. doi: 10.1016/j.agrformet.2013.02.003
5
6
7
8
9

Agricultural and Forest Meteorology 174–175 (2013) 43–53



The banner features the Elsevier logo on the left, a central text box with the journal title and homepage URL, and a small journal cover image on the right. The text in the central box reads: "Contents lists available at SciVerse ScienceDirect", "Agricultural and Forest Meteorology", and "journal homepage: www.elsevier.com/locate/agrformet".

Effect of spatial heterogeneity on the validation of remote sensing based GPP estimations



Gy. Gelybó^{a,b}, Z. Barcza^{b,c,+}, A. Kern^b, N. Kljun^d

^aInstitute for Soil Sciences and Agricultural Chemistry, Centre for Agricultural Research, Hungarian Academy of Sciences, H-1022 Budapest, Herman O. út 15, Hungary

^bDepartment of Meteorology, Eötvös Loránd University, H-1117 Budapest, Pázmány P. s. 1/A, Hungary

^cInstitute of Ecology and Botany, Centre for Ecological Research, Hungarian Academy of Sciences, H-2163 Vácrátót, Alkotmány u. 2-4, Hungary

^dDepartment of Geography, Swansea University, Singleton Park, Swansea SA2 8PP, United Kingdom

10

11 EFFECT OF SPATIAL HETEROGENEITY ON THE VALIDATION OF REMOTE
12 SENSING BASED GPP ESTIMATIONS

13

14 Gelybó, Gy.^{1,2}, Barcza, Z.^{2,3*}, Kern, A.², Kljun, N.⁴

15

16 ¹ Institute for Soil Sciences and Agricultural Chemistry, Centre for Agricultural
17 Research, Hungarian Academy of Sciences, H-1022 Budapest, Herman O. út 15,
18 Hungary

19 ² Department of Meteorology, Eötvös Loránd University, H-1117 Budapest, Pázmány
20 P. s. 1/A, Hungary

21 ³ Institute of Ecology and Botany, Centre for Ecological Research, Hungarian Academy
22 of Sciences, H-2163 Vácrátót, Alkotmány 2-4, Hungary

23 ⁴ Department of Geography, Swansea University, Singleton Park, Swansea SA2 8PP,
24 United Kingdom

25

26

27 Correspondence:

28 *dr. Zoltán BARCZA*

29 *Department of Meteorology*

30 *Eötvös Loránd University*

31 *H-1117 Budapest, Pázmány P. s. 1/A, Hungary*

32 *Phone: +36 1 372 2500 ext. 6603*

33 *Fax: +36 1 372 2904*

34 *E-mail: bzoli@elte.hu*

35 **Abstract**

36 Satellite based remote sensing provides an efficient way to estimate carbon balance
37 components over large spatial domains with acceptable temporal and spatial resolution.
38 In the present study remote sensing based gross primary production (GPP) estimations
39 were evaluated using data from a tall eddy-covariance flux tower, located over a
40 heterogeneous agricultural landscape in Hungary. Four different methods were used to
41 simulate 8-day mean GPP for the tower site based on the MOD17 light use efficiency
42 model. Additionally, we present a novel approach for model validation to exploit the
43 advantage of footprint size similarity between remote sensing and the hourly eddy
44 covariance signal measured at the tall tower. Besides using footprint information for the
45 model validation we performed downscaling of MOD17 using 250 m resolution
46 MODerate resolution Imaging Spectroradiometer (MODIS) Normalized Difference
47 Vegetation Index (NDVI) dataset in order to address land use heterogeneity. The results
48 showed that GPP was underestimated by MOD17 especially in years with average
49 precipitation during the growing season, while model performance was better during
50 dry years. Our downscaling technique significantly improved agreement between the
51 MOD17 model results and the eddy covariance measurements (modeling efficiency
52 (ME) increased from 0.783 to 0.884, root mean square error (RMSE) decreased from
53 $1.095 \text{ g C m}^{-2} \text{ day}^{-1}$ to $0.815 \text{ g C m}^{-2} \text{ day}^{-1}$), although GPP remained underestimated
54 (bias decreased from $-0.680 \text{ g C m}^{-2} \text{ day}^{-1}$ to $-0.426 \text{ g C m}^{-2} \text{ day}^{-1}$). Model evaluation
55 results suggest that model performance should be optimally evaluated using RMSE,
56 index of agreement (IA), ME and bias. The presented method is applicable to any eddy-
57 covariance tower with limitations depending of the complexity of landscape around the
58 flux tower. As incorporation of footprint information clearly impacts validation results,
59 future model validation and/or calibration should also involve source area estimation
60 which can be easily implemented following the presented approach.

61

62 **Keywords:** cropland, eddy covariance, footprint, light use efficiency model, MODIS

63 **1 Introduction**

64

65 Croplands occupy significant areas of the ice-free land surface (Foley et al., 2005)
66 including Europe (Wattenbach et al., 2010), and they are the dominant land-cover type
67 of many industrial countries, newly industrializing countries, as well as developing
68 countries (Ramankutty and Foley, 1999; Goldewijk, 2001; Ramankutty et al., 2002,
69 2008; Monfreda et al., 2008; Pittman et al., 2010). This means that croplands play a
70 significant role in the greenhouse gas (GHG) balance of the global land surface
71 (Bondeau et al., 2007).

72 Croplands are also among the most heterogeneous land cover types in many regions of
73 the world. Cropland heterogeneity is the consequence of rotations of crops with
74 different photosynthetic pathway (C3 or C4), farmland size and extent, occasional
75 abandonment of cultivated land, irrigation practices, application of manure or synthetic
76 fertilizers, harvest timing, and other management practices (Lobell and Asner, 2004;
77 Barcza et al., 2009a; Kutsch et al., 2010). Spatially representative, cropland specific
78 carbon balance estimations are crucial to constrain the greenhouse gas (GHG) balance
79 of regions with agriculture as the dominant land cover type (Bondeau et al., 2007;
80 Barcza et al., 2009b; Ciais et al., 2010). This represents a major challenge primarily
81 caused by cropland heterogeneity.

82 Direct field measurements based on the eddy covariance (EC) technique (Baldocchi,
83 2003) are widely used to assess the carbon balance of croplands (Suyker et al., 2005;
84 Kutsch et al., 2010; Gebremedhin et al., 2012; Wu et al., 2012). However, EC
85 measurements alone are unable to provide regional or country scale estimations because
86 of their limited spatial representativeness, which means that the results cannot be simply
87 upscaled (Wang et al., 2006; Barcza et al., 2009a). The available plot level
88 measurements can help to constrain the large scale estimations, e.g., through calibration
89 of ecosystem models (Braswell et al., 2005; Van Oijen et al., 2005; Hidy et al., 2011;
90 Ma et al., 2011). In spite of significant advances in biogeochemical modeling, carbon
91 balance estimations relying purely on process based models are usually highly uncertain
92 (Vetter et al., 2008; Schwalm et al., 2010; Wang et al., 2011).

93 One possible way to reduce uncertainty is to use state-of-the-art data-oriented models
94 (Ciais et al., 2010). Satellite based radiance measurements provide invaluable, high
95 accuracy information on the properties of land and ocean surfaces, and the atmosphere.
96 The radiances information can be used to construct sophisticated data-oriented models
97 that provide insight into several processes related to the environment (Turner et al.,
98 2004). Thanks to their global spatial coverage, remotely sensed data can provide
99 estimates for the carbon balance components on regional and continental scale, thus
100 they can be used as additional input for synthesis studies (Schulze et al., 2009; Ciais et
101 al., 2010). However, it is essential to evaluate and – if necessary – to improve the
102 performance of the remote sensing based models before applying them to larger spatial
103 scale (Turner et al., 2006; Heinsch et al., 2006).

104 In the present paper we focus on remote sensing based gross primary production (GPP)
105 estimates. The basic requirements for remote sensing based GPP simulation are the
106 following: 1) due to the dynamic nature of ecosystem functioning, satellite based
107 observations with relatively high temporal frequency are needed to detect changes in
108 productivity and phenological state (especially in case of agroecosystems); 2) the spatial
109 resolution of the remote sensing based observations should be comparable with the
110 footprint extent of the available, ground based measurements; 3) the spatial resolution

111 should also allow the upscaling to estimate regional, country, continental or global scale
112 studies (Running et al. 1999a).

113 As a compromise between spatial and temporal resolution of remotely sensed data,
114 information from the MODerate resolution Imaging Spectroradiometer (MODIS)
115 sensors (onboard the National Aeronautic and Space Administration Earth Observing
116 System (NASA EOS) Aqua and Terra satellites) are frequently used to construct data-
117 oriented GPP models. The MOD17 product (which is one of the official MODIS
118 products disseminated by NASA Earth Observing System Data and Information System
119 (EOSDIS)) is widely used in biogeochemical research which provides GPP data in 1 km
120 resolution with global coverage (Running et al., 1999b).

121 Results of the EC measurements are widely applied for the evaluation of MOD17 based
122 estimations of ecosystem scale carbon balance components (Leuning et al., 2005;
123 Gebremichael and Barros, 2006; Heinsch et al., 2006; Turner et al., 2006; Zhang et al.,
124 2008; Kanniah et al., 2009; Chasmer et al., 2011; Chen et al., 2012). Measurement-
125 model differences are frequently recognized by the validation studies. If the EC
126 instruments are mounted at ~5-30 m height above the canopy top (we refer to those flux
127 towers as “small” towers), the flux footprint is usually smaller than the 1 km spatial
128 resolution of the MOD17 model (at least for daytime, unstable stratification when the
129 satellite measurements take place; Göckede et al., 2008). This means that discrepancies
130 between measurements and model results can partly be caused by the mismatch in
131 spatial representativeness of the remote sensing and flux tower measurements (Schmid
132 and Lloyd, 1999; Turner et al., 2005; Kim et al., 2006; Chasmer et al., 2011). Following
133 this logic it can be hypothesized that tall tower based EC measurement results should be
134 in better agreement with estimations from remote sensing data, because the scale of
135 their spatial representativeness is similar (Barcza et al., 2009a), although land cover
136 heterogeneity is expected to have more influence on EC measurements in this case.
137 The agreement of model results and observations is usually also affected by land
138 use/land cover heterogeneity (Turner et al., 2005). For example, Göckede et al. (2008)
139 showed that in the CARBOEUROPE-IP network only one third of the flux sites are
140 located in homogeneous terrain, which means that a relatively large number of EC sites
141 are not ideal for remote sensing based model validation.

142 Measurement-model deviation can also be caused by the special location of the flux
143 tower relative to the 1 km resolution MOD17 grid cells, which means that information
144 from more than one pixel should be considered for the proper interpretation of the
145 results. This problem is generally addressed by simply averaging e.g. 3×3 or 5×5
146 MOD17 pixels for the validation (e.g. Turner et al., 2005; Chasmer et al., 2011). As an
147 example, limitations imposed by the different spatial representativeness of small EC
148 tower and satellite based measurements were addressed in a similar fashion within the
149 Bigfoot project (Reich et al., 1999; Turner et al., 2005). Within Bigfoot, EC
150 measurements over different land cover types (cropland, hardwood forest, coniferous
151 forest, boreal forest, tundra and grassland) have been scaled up to 5×5 km using a
152 process based ecosystem model in order to compare with MOD17 GPP/NPP
153 estimations. The study was based on small tower measurements, and footprint impacts
154 have not been incorporated.

155 Recent studies linking MOD17 data with EC measurements using footprint information
156 have been limited to small flux towers over forests (Chen et al., 2008, 2009; Chasmer et
157 al., 2011). No similar study exists for tall tower measurements over croplands to the

158 knowledge of the authors in spite of the large footprint area of tall towers (Wang et al.,
159 2006; Barcza et al., 2009a).
160 Our main aim is to validate MOD17 GPP over croplands and to improve the
161 methodology of remote sensing based GPP validation for eddy covariance towers. The
162 method is demonstrated and evaluated at Hegyhátsál tall tower site (Hungary). The
163 study site is ideal to test our hypothesis that remote sensing and EC measurements can
164 be synchronized since (i) the tall flux tower's footprint is comparable to MODIS spatial
165 resolution (EC sensors are mounted at 82 m height above the surface; see Barcza et al.
166 2009a), (ii) the tower is located within a heterogeneous agricultural landscape providing
167 realistic spatial and temporal variability of ecosystem carbon exchange. Rapid changes
168 of tower footprint locations due to varying meteorological conditions are considered in
169 our approach, which means that the MOD17 GPP model results are combined with
170 estimated footprint locations calculated from the available hourly flux data (Barcza et
171 al., 2009a). Due to the heterogeneity of land cover around the tall EC tower, the 1 km
172 resolution of the GPP model might smooth out small scale effects that influence the EC
173 measurements. In order to find a better match between the spatial representativeness of
174 the hourly EC measurements and remote sensing we introduce a new approach, where
175 the MOD17 model is downscaled to a 250 m grid (corresponding to the MODIS
176 Normalized Difference Vegetation Index (NDVI) product). This downscaling is also
177 necessary because of the size of the individual agricultural fields surrounding the tower
178 where the parcels represent homogeneous land cover type with similar spatial extent to
179 the 250 m NDVI product. The downscaled model is also evaluated using footprint
180 information derived from the EC measurements.
181 We would like to stress that the aim of the present study is to use exclusively MODIS
182 data as remote sensing information. The reason for this approach being the fact that
183 researchers have easy and straightforward access to this kind of data e.g. through the
184 FLUXNET website (ftp://daac.ornl.gov/data/modis_ascii_subsets/) or through EOSDIS
185 (NASA's Earth Observing System and Data and Information System
186 <http://earthdata.nasa.gov/>).

188 **2 Materials and methods**

190 **2.1 Site description**

191
192 A tall tower based eddy covariance system was established in Western Hungary near
193 village Hegyhátsál (46°57'21"N, 16°39'08"E 248 m asl) in 1997 with continuous
194 measurements of atmosphere/ecosystem CO₂ exchange (Haszpra et al., 2001, 2005).
195 The tower is surrounded by agricultural fields and forest patches (Barcza et al., 2009a).
196 The surrounding mosaic type land use is typical for Hungary as changes in property and
197 structure of farming systems in the last 20 years shifted the typical Hungarian farmlands
198 toward smaller fields and more complex cultivation patterns. The soil type in the region
199 is 'Lessivated brown forest soil' (Haplic Cambisol according to the WRB
200 classification). The soil texture is loam/silt loam.
201 The EC system is mounted at 82 m height which has a significant impact on the spatial
202 representativeness of the tower (Barcza et al., 2009a). Due to the height of the tower,
203 hourly averaging is applied on raw EC data (Haszpra et al., 2001, 2005). For the present
204 study, six years data of net ecosystem exchange (NEE) measurements at the Hegyhátsál
205 tall tower from 2001 to 2006 have been selected in accordance with the availability of

206 remote sensing data (availability of MOD17 results was constrained by availability of
207 the meteorological reanalysis input dataset; M. Zhao, personal communication).
208 Climate data for the study period and the 1981-2010 reference period are presented in
209 Table 1. Annual precipitation varied considerably during the study years. The 2001-
210 2006 period can be separated to two subperiods: a dry and warm period in the beginning
211 (2001-2003), and a cool period with higher precipitation (2004-2006) with
212 meteorological characteristics closer to the longterm average. This feature provides a
213 good opportunity to test the model in contrasting environmental conditions.

214

215 2.2 Eddy covariance data processing and flux partitioning

216

217 In recent years, several gap filling methods have been suggested to gain defensible
218 annual sums of NEE (Falge et al., 2001; Moffat et al., 2007). Methods used for gap
219 filling are also frequently used for the partitioning of NEE into gross primary
220 production and total ecosystem respiration (R_{eco}). In flux partitioning at daily time step,
221 first R_{eco} is determined and GPP is calculated as the signed difference between NEE and
222 the total daily R_{eco} .

223 As direct validation of daytime ecosystem respiration and GPP is not possible, the
224 uncertainty of flux partitioning results can be quite large (Lasslop et al., 2009). One way
225 to reduce this uncertainty and to provide a robust estimate of GPP is to apply several
226 gap filling and flux partitioning (GF/FP) methods. As an example, Lasslop et al. (2009)
227 recommended the combined use of two GPP/ R_{eco} separation methods to assess
228 uncertainty in the GPP estimations, and the authors also suggested the application of
229 additional methods for GPP/ R_{eco} separation. Following the logic of Lasslop et al. (2009)
230 here we applied three GF/FP methods discussed in Stoy et al. (2006), namely the Short
231 Term Exponential (STE, Reichstein et al., 2005), the Rectangular Hyperbolic (RH) and
232 the Non-Rectangular Hyperbolic (NRH, Gilmanov et al., 2003) methods.

233 In the STE method, hourly R_{eco} is determined using a temperature dependent respiration
234 function (estimated exclusively from nighttime NEE, which is assumed to be equal to
235 total ecosystem respiration) of the soil/vegetation system (Lloyd and Taylor, 1994). The
236 Lloyd and Taylor function is used to estimate daytime ecosystem respiration (Reichstein
237 et al., 2005). However, the STE method can lead to misinterpretations when applying it
238 to tall tower data. The determined relationships using nighttime fluxes might not be
239 applicable to daytime data since the nighttime source area can be much larger than the
240 daytime one, thus different regions can be ‘seen’ through the course of the day (Horst
241 and Weil, 1992; Wang et al., 2006). Moreover, prevailing wind can be different during
242 night and day (Barcza et al., 2003), thus land cover heterogeneity and anthropogenic
243 emission could also have different effects on the nighttime and daytime fluxes. The
244 footprint mismatch problem may cause bias in the estimated GPP results based on STE.
245 In the RH and NRH methods R_{eco} estimates are retrieved from daytime NEE data
246 (Gilmanov et al., 2003), therefore they are appropriate methods to be used for flux
247 partitioning of tall tower data. Applicability of the RH and NRH method is also
248 supported by Stoy et al. (2006) where the authors found that GPP estimated using the
249 NRH method matched best with independent estimates across different biomes.
250 Rectangular hyperbolic and non-rectangular hyperbolic functions (so-called light
251 response curves) are used to describe the relationship between hourly daytime NEE and
252 photosynthetic photon flux density (PPFD) and to determine daytime average rate of

253 respiration (R_d). The RH and NRH methods only differ in the mathematical
 254 representation of the fitted function. RH method uses the following formulae:
 255

$$256 \quad NEE = -\frac{a b \text{PPFD}}{(b + \text{PPFD})} + R_d, \quad (1)$$

257 while NRH uses another equation:
 258

$$259 \quad NEE = -\frac{a \text{PPFD} + b - \sqrt{(a \text{PPFD} + b)^2 - 4abc \text{PPFD}}}{2c} + R_d. \quad (2)$$

260 a , b and c are parameters determined by nonlinear (Levenberg-Marquardt least-squares
 261 minimization) regression process.
 262 Because of the relatively small number of available daytime NEE measurements (due to
 263 hourly averaging and data gaps) and the scatter of tall tower data, NEE data from a
 264 period of maximum 10 days was used in curve fitting instead of daily time step that is
 265 typically applied for short flux tower data (Gilmanov et al., 2003). Part of the
 266 information about day-to-day variations of relationships between NEE and
 267 environmental parameters can be lost due to the relatively long time window, but as
 268 model validation is performed with 8-day averaging of GPP, accurate representation of
 269 the day-to-day variability has less importance.
 270 In the two light response curve methods (RH and NRH) hourly ecosystem respiration is
 271 calculated in a second step, based on daytime average rate of respiration. R_d data of a
 272 given period (minimum 10 data points covering minimum 15°C temperature range)
 273 were used to construct temperature dependent functions. Hourly R_{eco} was calculated
 274 based on the temperature- R_d function and hourly temperature measurements.
 275 Best estimate for daily GPP was obtained as the mean of the results from the three
 276 GF/FP methods (Lasslop et al., 2009; Beer et al., 2010). Mean GPP obtained from tall
 277 tower measurements is referred as “GPP-tower”. Uncertainty arising from GF/FP
 278 procedure is estimated as half of the difference between the daily maximum and
 279 minimum GPP estimate (Beer et al., 2010).
 280

281

282

283 2.3 Modeling approach

284

285 2.3.1 The MODIS GPP (MOD17) remote sensing based model

286

287 The MOD17 product provides global GPP estimates of 8-day temporal and 1 km spatial
 288 resolution (Running et al., 1999b; Heinsch et al., 2003). The underlying GPP model of
 289 the MOD17 product (the ‘MOD17 model’) is based on the light use efficiency approach
 290 (Monteith 1972, 1977). The model can distinguish 11 biome categories (Plant
 291 Functional Types, PFTs), including one agricultural category (‘croplands’). PFT
 292 specific model parameters, i.e. values of light use efficiency (ε_{max} , kg C MJ⁻¹), and
 293 parameters describing environmental (meteorological) stress factors are stored in the
 294 biome properties look-up table (BPLUT) for each PFT. These parameters do not vary
 295 with geographical location for a given PFT; they characterize biomes on a global scale.
 296 Input data requirements of the MOD17 model include land cover information (MOD12
 297 land cover product; Strahler et al., 1999), fraction of absorbed photosynthetically active

298 radiation (MOD15 LAI/FPAR product; Knyazikhin et al., 1999), meteorological data
299 (NASA Global Modeling and Assimilation Office (GMAO) reanalysis dataset): global
300 radiation (GR, MJ m⁻² day⁻¹), minimum temperature (T_{min}, °C), vapor pressure deficit
301 (VPD, Pa).
302 Different GPP model setups were used in this study, all of them based on MOD17
303 version 5.1 official data product, kindly provided by Numerical Terradynamic
304 Simulation Group, University of Montana (UMT NTSG).

305

306 2.3.2 Processing of remote sensing data

307

308 The MOD15 FPAR/LAI MODIS product (UMT NTSG version 5) served as remote
309 sensing input data for the MOD17 model. For quality assurance of FPAR data (quality
310 flag based data selection and interpolation) we followed description provided by Zhao et
311 al. (2006). These FPAR data are used as remote sensing input for most model runs in
312 this study (see below).

313 Preprocessed, 250 m resolution NDVI data were also used in this study for GPP
314 calculations. NDVI preprocessing steps have been previously documented in Barcza et
315 al. (2009a). Here we provide a short description of the methodology used to construct
316 daily temporal resolution NDVI courses. For detailed information on NDVI quality
317 assurance, processing and analysis see Barcza et al. (2009a).

318 The NDVI analysis uses the 250 m resolution MOD13 vegetation index product (Huete
319 et al., 1999) constructed from the multispectral information provided by the MODIS
320 sensor. First, an area comprising 41×41 pixels surrounding the tower has been selected.
321 In order to minimize the errors in NDVI time series, quality control of NDVI time series
322 of all 250 m NDVI pixels were filtered and smoothed using wavelet transformation.
323 Two basic crop types have been separated based on their typical annual NDVI courses.
324 It has been concluded from the analysis that winter crops (typically winter wheat) and
325 summer crops (typically maize) are both present in the vicinity of Hegyhátsál tower.
326 The resulting daily resolution NDVI courses were used in this study to retrieve FPAR.
327 The actual input for the modified MOD17 model was calculated following Sims et al.
328 (2005):

$$329 \quad FPAR = 1.24NDVI - 0.168. \quad (3)$$

330 For simplicity, we use this simple linear approach rather than the more sophisticated
331 retrieval of the official 1 km resolution FPAR product, or the nonlinear backup
332 algorithm for MODIS FPAR (Knyazikhin et al., 1999). Note that the Sims et al. (2005)
333 formula provides somewhat lower FPAR estimates than the MOD15 backup algorithm.

334

335 2.3.3 Footprint modeling

336

337 Synchronizing the spatial representativeness of remote sensing and EC based GPP
338 estimations requires combined information on crop type and phenological state
339 (obtained from NDVI above) and the dynamic variation of the source area.

340 The actual source area of the vertical CO₂ flux measured by the EC system can be
341 estimated using a footprint model. In the present study the simple, parameterized
342 footprint model of Kljun et al. (2004) was used (their Eqs. 17 and 11). Based on remote
343 sensing information, objective crop classification, footprint modeling and separation of
344 NEE signal according to crop types, Barcza et al. (2009) showed that the Kljun et al.
345 (2004) footprint parameterisation (based on the Lagrangian footprint model of Kljun et

346 al., 2002) provides accurate estimates for maximum source weight locations. In order to
347 propose a simple yet powerful method for footprint analysis only the maximum source
348 weight location (zero dimension information) are used exclusively to assign surface
349 elements to the measured signal (using the approach of Barcza et al., 2009). The surface
350 elements are defined by the 250m resolution NDVI grid provided by MOD13. Fig. 1
351 shows the footprint climatology of the site for year 2007. It is clear from the plot that
352 several 250m resolution pixels contribute to the measured signal, and it is also clear that
353 such coarse resolution grid can be used to differentiate between the contributing surface
354 elements.

355

356

357 2.4 Model formulation

358

359 Discrepancies between GPP derived from EC tower measurements and MOD17
360 estimates can be either caused by errors in the input data or originate from the structure
361 of the model (including uncertainty in model parameters) (Running et al., 2004;
362 Nightingale et al., 2007; McCallum et al., 2009), or by mismatch of EC validation data
363 and remote sensing information. We performed calculations with different model setups
364 (i) to examine and eliminate the effect of possible errors in the input data and (ii) to
365 resolve spatial representativeness issues. Our primary aim is not to improve model
366 performance by the modification of model structure or parameters, but to explore the
367 main causes of model-measurement discrepancy that can affect the result of validation
368 studies. An overview of main properties of these model setups is given in Table 2.
369 Detailed description of each modeling experiment is given in the following. All
370 calculations are performed on a daily temporal resolution and then summed for 8-day
371 average values.

372

373 1) GPP-GMAO (reference run)

374

375 We adapted the MOD17 model algorithm (MOD17 User's guide; Zhao et al., 2005) and
376 performed simulations with original settings and input data (GMAO meteorology,
377 MOD15 LAI/FPAR product Collection 5.1, MOD12 land cover information, BPLUT
378 version 5.1; M. Zhao, personal communication). Our implementation was found to be in
379 a good agreement with the official version 5.1 MOD17 product ($R^2 = 0.99$ and bias =
380 $-0.018 \text{ g C m}^{-2} \text{ year}^{-1}$ for the examined six years). The slight deviance between our
381 implementation and the official product is most likely caused by the quality assurance
382 of FPAR. In the following, we refer to this run as "GPP-GMAO", and consider it to be
383 equivalent with the official MOD17 product. Note that only the 1 km MODIS pixel
384 containing the measurements site is considered in this setup and is compared with tower
385 based GPP.

386

387 2) GPP-met (modification of meteorological input)

388

389 The MOD17 model has been shown to be sensitive to the meteorological input dataset
390 (Running et al., 2004; Zhao et al., 2006). To address this issue we replaced the global
391 meteorological reanalysis data with local (on-site) meteorological measurements (vapor
392 pressure deficit and global radiation, daily minimum temperature). The MT-CLIM
393 model was used to fill the gaps in the local meteorological measurements (Thornton et

394 al., 2000). We refer to these estimations as “GPP-met”. Similarly to GPP-GMAO, the
395 1 km MODIS pixel containing the flux tower is used for validation.

396
397 3) GPP-FP (simple representation of tower footprint)

398
399 To address heterogeneity in the vegetation cover, FPAR data at 1 km resolution was
400 extracted according to the actual flux footprint (we refer to this method as “GPP-FP”).
401 According to the footprint climatology presented in Fig. 1, the 1 km resolution already
402 enables differentiation in the source region. This is a rough consideration of the
403 dynamic variations of the source area in time especially in a region where typical size of
404 agricultural parcels is still in the subpixel range (around 200 m), but a first step to
405 synchronize representativeness of remote sensing and eddy covariance measurements.
406 At flux towers where the land cover heterogeneity is not realized as random patches of
407 different PFTs or crop types, but as different land cover types in well-defined directions
408 from the tower, this method can provide sufficient background for the interpretation of
409 eddy covariance measurements.

410
411 4) GPP-NDVI (downscaling MOD17 using 250 m resolution NDVI data)

412
413 It has been shown in Barcza et al. (2009a) that different locations (agricultural fields)
414 over the heterogeneous landscape surrounding the tower do not have identical
415 contributions to the measured signal (Fig. 1), therefore a mismatch between
416 representativeness of the remotely sensed data and EC measurements inevitably occurs.
417 In order to (i) account for land cover heterogeneity, and (ii) synchronize the
418 representativeness of the GPP model and the tower, we developed a new methodology.
419 Firstly, instead of using the 1 km resolution MOD15 FPAR, we applied a downscaling
420 procedure using the 250 m MODIS NDVI time series and known relationship between
421 FPAR and NDVI. Downscaling of model calculations is supposed to answer the
422 question whether the coarse spatial resolution of the FPAR product is responsible for
423 model inaccuracies to a certain degree.

424 Secondly, the use of the 250 m spatial resolution NDVI dataset offers the possibility of
425 taking into account both the hourly footprint of the tower measurements (following
426 Kljun et al., 2004) and the phenology of the individual fields with finer resolution. This
427 is expected to result in improved differentiation of winter and summer crop phenology
428 instead of modeling them as a fictional “average crop”.

429 These modeling efforts are substantially based on the estimated spatial
430 representativeness of the tall tower described in Barcza et al., (2009a). The discretized
431 hourly footprint locations (for selection of the NDVI pixel location as primary
432 sink/source location of CO₂ flux), together with the according daily NDVI data from the
433 smoothed NDVI curve of the selected pixel are combined in GPP calculations (see
434 Section 2.3.2 NDVI data preprocessing).

435 Suppose that according to the footprint model on the i^{th} day of the year the number of
436 pixels that contributed to the measured flux was P (out of the 41×41 pixels; see Section
437 2.3.2). FPAR_i^p denotes the FPAR value of the p^{th} individual pixel on the i^{th} day and is
438 calculated from the according daily NDVI value (NDVI_i^p).

439 Following the scheme of the MOD17 model (Running et al., 1999b), GPP of this pixel
440 can be derived as:

441

$$442 \quad \text{GPP}_i^p = W_i^p \text{ FPAR}_i^p \text{ IPAR } \varepsilon_i. \quad (4)$$

443

444 Here W_i^p is the weight of each contributing pixel (here calculated as the number of

445 hours in the i^{th} day when the source area was located at the p^{th} pixel),

446 $\varepsilon_i = \varepsilon_{\max} f(T_{\min_i}) f(\text{VPD}_i)$ is the actual light use efficiency, and $\text{IPAR} = 0.45 \text{ GR}_i$.

447 Daily GPP on the i^{th} day is calculated from the weighted average of GPP of the

448 contributing pixels:

$$449 \quad \text{GPP}_i = \frac{\sum_{p=1}^P \text{GPP}_i^p}{\sum_{p=1}^P W_i^p}. \quad (5)$$

450

451 The footprint information is not always available for each hour of the day (when the
452 footprint model does not provide result). Therefore the GPP calculation might be biased
453 because it can only rely on available footprint location information.

454 The CORINE2000 land cover database (Büttner et al., 2002) re-gridded to the

455 250×250 m NDVI grid provides the land cover information to assist the selection of the

456 appropriate BPLUT category (Barcza et al. 2009a). Note that introduction of CORINE

457 based land cover data was necessary for the downscaling to 250 m. In our approach the

458 land cover categories retrieved in Barcza et al. (2009a) were comparable to MOD12

459 classification scheme. Therefore, discrepancies between model runs using MOD12 and

460 MODIS-NDVI due to misclassification of land cover are unlikely to occur. Moreover,

461 as the source area of CO_2 flux is attributed to croplands in $\sim 80\%$ of the cases for the

462 selected years, land cover classification can not have significant effect on the results.

463 The resulting dataset is referred to as ‘‘GPP-NDVI’’.

464

465

466 2.5 Evaluation of model performance

467

468 For statistical evaluation of different model simulations several indices were used. The

469 root mean square error (RMSE), bias, index of agreement (IA), modeling efficiency

470 (ME), Kendall correlation coefficient (KR) and Pearson linear correlation coefficient

471 (R^2) (Janssen and Heuberger, 1995; Ma et al., 2011) were calculated for each year

472 separately and for the whole study period as well. These indices can be considered as

473 measures of model ‘goodness’ from different aspects, thus behavior of the different

474 indices will allow characterizing model efficiency from different aspects.

475 RMSE measures the average absolute error in a quadratic sense; therefore it is sensitive

476 to outliers. In unbiased estimations, RMSE is the standard deviation. RMSE has the

477 same unit as the estimated parameter. Bias (or mean bias) describes the average

478 deviation between the model results and measurements, and is zero for unbiased

479 estimations. IA varies between 0 and 1 and describes a standardized measure of mean

480 square error. The closer IA is to 1 (ideal agreement) the better our estimation is. IA is

481 0.4 for two random series therefore IA should be over 0.4 for two correlated variables.

482 ME ranges between $-\infty$ to 1, and gives the improvement in estimations compared to the

483 mean of the observation. Any positive ME suggests improvement, but closer to 1 is

484 better. KR and R^2 describe the association between observation and model predictions.
485 Both indices vary between -1 and 1 (perfect agreement), and are zero when there is no
486 agreement between the datasets. R^2 assumes linear dependence between the variables,
487 while KR does not require linear relationship (KR does not have any assumption about
488 the distributions of the variables).
489 Because GPP-NDVI was only available from 2003 (year after the launch of Aqua
490 satellite), model performance was characterized for the whole 2001-2006 period where
491 possible, and for 2003-2006 as well in case of GPP-GMAO, GPP-met and GPP-FP.

492
493
494
495

3 Results

496 GPP-GMAO estimations and the GPP calculated from tall tower measurements (GPP-
497 tower) are shown in Fig. 2a. Overall, model results underestimate GPP obtained from
498 tall eddy covariance tower measurements. It can be seen that for the first three years
499 (2001-2003) the model results are in good agreement with tower GPP. However, for the
500 last three years (2004-2006), the measured GPP increased significantly. GPP-GMAO,
501 however, remained at similar levels throughout the study period (2001 – 2006). The
502 highest GPP-GMAO values barely exceed $6 \text{ g C m}^{-2} \text{ day}^{-1}$ while measured GPP is above
503 $8 \text{ g C m}^{-2} \text{ day}^{-1}$ in some periods. Higher measured GPP in 2004-2006 is caused by the
504 higher precipitation during the vegetation season (Table 1; see also Haszpra et al.,
505 2005), which provided favorable conditions for plant growth.

506 Results of statistical evaluation of the model performance for the whole study period are
507 presented in Table 3. The evaluation of the model performance shows reasonable
508 agreement with measured data both during the whole measurement period and the 2003-
509 2006 subperiod. However, GPP-GMAO annual sums underestimate GPP-tower in each
510 year (Fig. 3), and the underestimation increases toward the end of the investigated
511 period, exceeding $500 \text{ g C m}^{-2} \text{ year}^{-1}$ in 2006 (i.e. underestimation by nearly 40 %).
512 Note that in the second half of 2006 a large measurement gap occurred where the gap
513 filled GPP (not shown in Fig. 2) was higher than simulated GPP, therefore tower based
514 annual total may be biased.

515 For GPP calculations based on local meteorological measurements instead of GMAO
516 reanalysis, model performance slightly improved (GPP-met in Table 3). Although
517 RMSE increased compared to GPP-GMAO, correlation increased as KR and R^2 values
518 suggest. Interannual variability of the statistical parameters is presented in Fig. 4. The
519 improvement in model performance was not consistent for all years and for all
520 parameters. When changing meteorological input data, correlation coefficient values
521 (KR and R^2) increased, but RMSE, IA and ME do not show such a systematic pattern
522 (Table 3). Annual totals are underestimated again, even more than for GPP-GMAO
523 results (Fig. 3). According to Fig. 2b, in spite of the bias in magnitude of annual sums,
524 daily GPP totals reach higher peak values than GPP-GMAO though still remaining well
525 below measured peak daily sums.

526 Tracking footprint location on 1 km resolution in GPP-FP runs only slightly improved
527 model agreement (Table 3). Annual totals got closer to flux tower based estimations
528 than GPP-met results, although compared to GPP-GMAO estimations the improvement
529 is not consistent in all years (Fig. 3). The statistical evaluation shows a similar pattern,
530 as most of the indices show improvement except for KR and R^2 which decreased
531 compared to both GPP-GMAO and GPP-met (Table 3).

532 Model performance further improved when NDVI based downscaling integrated with
533 footprint information was applied (GPP-NDVI). RMSE and model agreement
534 parameters (especially ME and bias) show the best results among all model runs in most
535 years of the test period (Fig. 4, Table 3). Annual totals are closer to GPP-tower sums but
536 again, model simulations underestimate measured GPP and were barely able to describe
537 interannual variability (Fig. 3).
538 Modifications in model setup gradually improved model performance compared to
539 measurements. However, different indicators suggest different degree of improvement.
540 Certain indicators such as RMSE, IA, ME and bias showed significant and systematic
541 improvement especially in case of GPP-NDVI, while KR and R^2 coefficients do not
542 differ significantly among model runs (Fig. 4).

543

544 **4 Discussion**

545

546 Overestimation and underestimation of flux tower GPP by MOD17 have been
547 extensively reported in the literature. Among possible causes, several factors have been
548 discussed, such as effect of meteorological input data (Heinsch et al., 2006), or
549 differences in spatiotemporal coverage (Heinsch et al., 2006; Yang et al., 2007).
550 According to literature, in the case of croplands, MOD17 has a systematic negative bias,
551 and the underestimation is especially pronounced at high productivity sites. Yang et al.
552 (2007) found an average error of 50.3% for non-forested ecosystems, with the largest
553 underestimation (61%) for cropland (irrigated maize, USA). The identification of the
554 sources of these errors is critical to understand the limitations of the model and also to
555 improve its performance especially over heterogeneous croplands.

556

557 4.1 The effect of GPP model parameterization and meteorological input data

558

559 As a possible source of model error, accuracy of input meteorological data was
560 examined and compared to measurements at Hegyhátsál tall tower site. Global radiation
561 and minimum temperature estimations of GMAO are in a good agreement with
562 measurements (with RMSE of $3.23 \text{ MJ m}^{-2} \text{ day}^{-1}$ and 2.8°C and R^2 of 0.92 and 0.93,
563 respectively). This agreement does not vary among years to an extent which could
564 explain the underestimation of GPP in 2004-2006 (Fig. 2). However, VPD is
565 overestimated by GMAO and it was found that the error is pronounced in the last three
566 years (Table 1). This finding contradicts previous results in the literature, where GMAO
567 provided lower estimates for VPD when compared with data measured at flux towers,
568 and it has been proposed that spatial averaging of meteorological data causes the
569 discrepancy (Running et al., 2004; Turner et al., 2005). However, Hegyhátsál area is a
570 relatively wet part of the region, therefore spatial averaging might have increased VPD
571 as influenced by dryer areas in the same pixel. Overestimation of VPD has been shown
572 by Gebremichael and Barros (2006) for a humid tropical site, while Kanniah et al.
573 (2009) found overestimation in dry season and underestimation in wet season in case of
574 a tropical savanna.

575 If VPD is responsible for the discrepancies between GPP-tower and GPP-GMAO in
576 2004-2006, the results are supposed to match better if we use local meteorological
577 measurements. However, in spite of using local meteorological measurements, GPP
578 remained underestimated (Fig. 2b).

579 It is clear from Figs. 2a and 2b that differences in meteorological data affect the short
580 term variation of the model results, but are not responsible for the substantial difference
581 between model results and measurements.

582 The impact of meteorological data on the MOD17 model has been shown to be site-
583 specific, and sometimes, like in our case, the use of local measurements tends to
584 decrease the estimations of annual GPP sums (Heinsch et al., 2006; Running et al.,
585 2004) (Fig. 3). GPP-met runs provide very similar or slightly lower estimates compared
586 to GPP-GMAO, hence it can be concluded that errors in meteorological input data are
587 not the primary sources of underestimation of GPP. Underestimated maximum light use
588 efficiency (ϵ_{\max}) parameter together with the lack of soil water availability stress
589 parameterization (Hwang et al., 2008) could explain this behavior of the model. While
590 the first condition results in an underestimation of flux measurements in wet years, the
591 insufficient consideration of moisture stress cannot constrain GPP in dry years.
592 Consequently, the model provides more or less the same estimations both in wet and dry
593 years (Fig. 3). It suggests that the underestimation of light use efficiency is the key
594 factor resulting in a systematic negative bias. (However, this is not necessarily the case
595 with other biomes; see Turner et al. 2006; Heinsch et al. 2006.)

596 These findings are also supported by earlier studies presented in the literature. Zhang et
597 al. (2008) evaluated the MOD17 model using both GMAO reanalysis and local
598 meteorological measurements over cropland (winter wheat – maize crop rotation) and
599 an alpine meadow. They found significant underestimation by MOD17 results
600 particularly in case of the cropland site regardless of the meteorological data they used
601 as model input, and they suggested that the underestimation of ϵ_{\max} is mostly
602 responsible for the poor performance of MOD17.

603 The hypothesis about the trade-off between the effects of underestimated ϵ_{\max} and
604 insufficient moisture constraint is also supported by Coops et al. (2007). Evaluation of
605 the standard and modified MOD17 model runs have been carried out in this case using
606 site specific ϵ_{\max} in the first step combined with a soil water modifier (initially proposed
607 by Leuning et al., 2005) in the second step. They found underestimation by the standard
608 MOD17 algorithm, and an overestimation using site specific ϵ_{\max} . The overestimation
609 decreased when the soil moisture modifier was included in the MOD17 model resulting
610 in the highest agreement with measurements. Their findings hence suggest a combined
611 effect of errors in ϵ_{\max} and the water stress parameterization.

612

613 4.2 The impact of the footprint analysis on low spatial resolution input

614

615 Tracking footprint locations at 1 km resolution improved model performance. However,
616 GPP-FP still underestimates tower-based GPP estimations (Fig. 2c, Fig. 3). In the
617 comparison of remote sensing based GPP estimations and eddy covariance
618 measurements over a heterogeneous landscape the consideration of source area location
619 should improve model-measurement agreement to draw a more realistic picture of
620 model performance. In the present study, individual agricultural plots are typically
621 subpixel sized, therefore differences between remote sensing and EC measurements can
622 still occur as a result of spatial averaging. The different maximum light use efficiency
623 parameters attributed to different crop types together with the typical field size raises
624 the need for a downscaling of the model to benefit from footprint information.

625

626 4.3 Evaluation of the downscaling procedure combined with footprint analysis

627

628 Fig. 2d shows that GPP increased for GPP-NDVI and the magnitude of simulated GPP
629 is very well captured also in the 2004-2006 time period when precipitation was higher.
630 The increase in annual sums can also be seen in Fig. 3, however, the large difference
631 between GPP-NDVI and GPP-tower annual totals may be biased (see Section 3).
632 Though the tower is mainly surrounded by winter wheat (C3) and maize (C4),
633 differences in the properties of C3 and C4 crops are not reflected in GPP courses
634 although, as it can be seen from GPP-tower, C4 plants have higher light use efficiency
635 and thus higher maximum CO₂ uptake. Note that our novel downscaling method can
636 only eliminate errors in FPAR arising from spatial resolution and representativeness of
637 the remote sensing measurements. Structural problems of the model, i.e. poor
638 characterization of crop types cannot be resolved by this algorithm.
639 The analysis of statistical indices (Table 3) revealed that short term variability of
640 simulated GPP is mainly caused by variability of the meteorological parameters (T_{\min} ,
641 VPD). As our modifications mainly address the shortcomings of the coarse resolution
642 FPAR dataset, the explained variance is expected to remain basically unchanged. This
643 means that model performance of GPP should be optimally evaluated using RMSE, IA,
644 ME and BIAS, but not R^2 and KR. Future developments that might try to include e.g.
645 soil moisture and other stress factors are supposed to involve improvements in R^2 and
646 KR.

647

648

649 **5 Concluding remarks**

650

651 We presented a method for the adaptation and validation of the MOD17 light use
652 efficiency model for a tall tower based eddy covariance site located within
653 heterogeneous cropland in Hungary. The research is based on the previous footprint
654 analysis and crop phenology characterization by means of NDVI analysis (Barcza et al.,
655 2009a).

656 Four different methods were used to simulate 8-day mean GPP for Hegyhátsál based on
657 MODIS data. GPP-GMAO and GPP-met (GPP calculated using the MOD17 algorithm
658 using GMAO meteorology and local meteorological measurements) are widely used in
659 MOD17 related validation studies (e.g., Leuning et al., 2005; Heinsch et al., 2006;
660 Turner et al., 2006). In order to exploit the advantage of footprint size similarity
661 between remote sensing and hourly tall tower eddy covariance signal we further used
662 two refined methods. For the GPP-FP model setup the 1 km resolution MOD17 data
663 was coupled with the footprint analysis which allowed selection of MOD17 pixels
664 according to the prevailing meteorological conditions and turbulence conditions. For
665 GPP-NDVI we used the 250 m resolution MODIS NDVI dataset to downscale GPP
666 estimations to 250 m resolution. The downscaled model was also coupled with the
667 footprint analysis to provide hourly varying source region for the measured GPP. Note
668 that for the selection of the contributing surface elements we used the maximum source
669 weight location of the footprint model. This approach was shown to provide good
670 results for the Hegyhátsál tall tower (Barcza et al., 2009b).

671 The results showed that GPP-met and GPP-FP cause only modest improvements in
672 model performance compared to the reference GPP-GMAO. However, we demonstrated
673 that our new downscaling technique used in GPP-NDVI at 250 m resolution is

674 significantly more successful in modeling GPP at the typically heterogeneous landscape
675 of sub-pixel sized croplands in Western Hungary than the conventional GPP-GMAO.
676 It was shown that the 250 m resolution NDVI dataset is suitable for the characterization
677 of the Hegyhátsál cropland region where agricultural fields are typically small. This
678 means that the presented method can theoretically also be used for shorter towers,
679 keeping in mind that the applicability may be restricted depending on the complexity of
680 landscape surrounding the flux tower.

681 Depending on the structure of farmlands in the area of interest, we propose to use the
682 NDVI based GPP modeling methodology for regional scale studies at 250 m or 1 km
683 resolution using the following input data and procedure: (i) Quality assurance and
684 wavelet transformation of MODIS NDVI time series that can be reproduced following
685 Barcza et al. (2009a), or quality controlled and interpolated NDVI time series calculated
686 using an alternative method (e.g., linear or spline interpolation). (ii) FPAR data
687 retrieved from NDVI (Eq. 3, cf. Sims et al., 2005); and (iii) meteorological data from
688 the GMAO database (until 2006) or a suitable meteorological database (e.g. from
689 national meteorological services) known to provide accurate results for the given region.
690 (iv) Derive GPP following the scheme of the MODIS GPP-model.

691 Applying the proposed method to our study site, annual GPP sums are still
692 underestimated (by ~18% in average in the vicinity of the Hegyhátsál tower), but the
693 underestimation is less than with the original MOD17 model. This means that validation
694 results are strongly affected by the joint interpretation of EC tower and remote sensing
695 data.

696 The presented methods allow for a more flexible utilization of remote sensing data for
697 simulation of crop phenology and productivity on local or regional scale over
698 heterogeneous landscape. As we pointed out, the choice of input datasets is important
699 for improving model accuracy. However, errors caused by poor characterization of the
700 ecosystem cannot be eliminated without calibration and/or structural improvement of
701 the LUE model. At least the physiological differences of winter crop (at our site
702 typically winter wheat, C3) and summer crop (typically maize, C4) should be included
703 in model parameterizations via calibration (cf. Chen et al., 2011). For Western Hungary,
704 the NDVI based crop type information (see Section 2.1.3) provides this possibility of
705 crop specific model runs and calibration of the MOD17 model.

706 Our results highlight that spatial representativeness issues can not be neglected when
707 validating remotely sensed GPP data with tall tower GPP data.

708 **Acknowledgements**

709

710 We are very grateful to Maosheng Zhao (NTSG) for providing us the official MOD17
711 product, the version 5.1 model parameters and the GMAO meteorological database. The
712 research is supported by the Hungarian Government and the European Union and
713 cofinanced by the European Social Fund (Jedlik Ányos PhD Candidate Fellowship,
714 project no. TÁMOP 4.2.4.A-1; and grant agreement no. TÁMOP 4.2.1/B-09/1/KMR-
715 2010-0003). The research was also supported by Hungarian Scientific Research Fund
716 (OTKA K101065, K104816), CarpathCC project (ENV.D.1/FRA/2011/0006), BioVel
717 (Biodiversity Virtual e-Laboratory Project, FP7-INFRASTRUCTURES-2011-2, project
718 number 283359), by GHG-Europe (Greenhouse gas management in European land use
719 systems, FP7-ENVIRONMENT, EU contract number 244122), and by the Natural
720 Environment Research Council (NERC) UK (NE/G000360/1). The eddy covariance
721 measurements were supported by the Hungarian Scientific Research Fund K75638 and
722 CK77550. Use of the TV-tower and transmitter building at Hegyhátsál is kindly
723 provided by Antenna Hungária Corporation. We thank Markus Reichstein for the
724 discussion about the possibility of joint use of eddy flux tower, footprint modeling and
725 MOD17 data.

726 **References**

727

- 728 Baldocchi, D.D., 2003. Assessing the eddy covariance technique for evaluating carbon
 729 dioxide exchange rates of ecosystems: past, present and future. *Global Change*
 730 *Biol.* 9, 479–492. doi:10.1046/j.1365-2486.2003.00629.x
- 731 Barcza, Z., Haszpra, L., Kondo, H., Saigusa, N., Yamamoto, S., Bartholy, J., 2003.
 732 Carbon exchange of grass in Hungary. *Tellus B* 55, 187–196. doi:10.1034/j.1600-
 733 0889.2003.00014.x
- 734 Barcza, Z., Kern, A., Haszpra, L., Kljun, N., 2009a. Spatial representativeness of tall
 735 tower eddy covariance measurements using remote sensing and footprint analysis.
 736 *Agric. For. Meteorol.* 149, 795–807. doi:10.1016/j.agrformet.2008.10.021
- 737 Barcza, Z., Haszpra, L., Somogyi, Z., Hidy, D., Lovas, K., Churkina, G., Horváth, L.,
 738 2009b. Estimation of the biospheric carbon dioxide balance of Hungary using the
 739 BIOME-BGC model. *Időjárás – Quarterly Journal of the Hungarian*
 740 *Meteorological Service* 113, 203-219.
- 741 Beer, C., Reichstein, M., Tomelleri, E., Ciais, P., Jung, M., Carvalhais, N., Rödenbeck,
 742 C., Arain, M.A., Baldocchi, D., Bonan, G.B., Bondeau, A., Cescatti, A., Lasslop,
 743 G., Lindroth, A., Lomas, M., Luysaert, S., Margolis, H., Oleson, K.W., Rouspard,
 744 O., Veenendaal, E., Viovy, N., Williams, C., Woodward, F.I., Papale, D., 2010.
 745 Terrestrial gross carbon dioxide uptake: global distribution and covariation with
 746 climate. *Science* 329, 834–838. doi:10.1126/science.1184984
- 747 Bondeau, A., Smith, P.C., Zaehle, S., Schaphoff, S., Lucht, W., Cramer, W., Gerten, D.,
 748 Lotze-Campen, H., Müller, C., Reichstein, M., Smith, B., 2007. Modelling the role
 749 of agriculture for the 20th century global terrestrial carbon balance. *Global Change*
 750 *Biol.* 13, 679–706. doi:10.1111/j.1365-2486.2006.01305.x
- 751 Braswell, B.H., Sacks, W.J., Linder, E., Schimel, D.S., 2005. Estimating diurnal to
 752 annual ecosystem parameters by synthesis of a carbon flux model with eddy
 753 covariance net ecosystem exchange observations. *Global Change Biol.* 11, 335–
 754 355. doi:10.1111/j.1365-2486.2005.00897.x
- 755 Büttner, G., Feranec, J., Jaffrain, G., 2002. Corine Land Cover Update 2000. Technical
 756 Report 89 (European Environment Agency, 2002) available at
 757 http://reports.eea.eu.int/technical_report_2002_89/en
- 758 Chasmer, L., Kljun, N., Hopkinson, C., Brown, S., Milne, T., Giroux, K., Barr, A.,
 759 Devito, K., Creed, I., Petrone, R., 2011. Characterizing vegetation structural and
 760 topographic characteristics sampled by eddy covariance within two mature aspen
 761 stands using lidar and a flux footprint model: Scaling to MODIS. *J. Geophys. Res.*
 762 116, G02026. doi:10.1029/2010JG001567
- 763 Chen, B., Black, T.A., Coops, N.C., Hilker, T., Trofymow, J.A., Morgenstern, K., 2008.
 764 Assessing Tower Flux Footprint Climatology and Scaling Between Remotely
 765 Sensed and Eddy Covariance Measurements. *Boundary-Layer Meteorol.* 130, 137–
 766 167. doi:10.1007/s10546-008-9339-1
- 767 Chen, B., Ge, Q., Fu, D., Liu, G., Yu, G., Sun, X., Wang, S., Wang, H., 2009. Upscaling
 768 of gross ecosystem production to the landscape scale using multi-temporal Landsat
 769 images, eddy covariance measurements and a footprint model. *Biogeosci. Discuss.*
 770 6, 11317–11345. doi:10.5194/bgd-6-11317-2009
- 771 Chen, B., Coops, N.C., Fu, D., Margolis, H.A., Amiro, B.D., Black, T.A., Arain, M.A.,
 772 Barr, A.G., Bourque, C.P.-A., Flanagan, L.B., Lafleur, P.M., McCaughey, J.H.,
 773 Wofsy, S.C., 2012. Characterizing spatial representativeness of flux tower eddy-

774 covariance measurements across the Canadian Carbon Program Network using
775 remote sensing and footprint analysis. *Remote Sens. Environ.*, 124, 742–755.
776 doi:10.1016/j.rse.2012.06.007

777 Chen, T., van der Werf, G.R., Dolman, A.J., Groenendijk, M., 2011. Evaluation of
778 cropland maximum light use efficiency using eddy flux measurements in North
779 America and Europe. *Geophys. Res. Lett.* 38, L14707.
780 doi:10.1029/2011GL047533W

781 Ciais, P., Wattenbach, M., Vuichard, N., Smith, P., Piao, S.L., Don, A., Luysaert, S.,
782 Janssens, I., Bondeau, A., Dechow, R., Leip, A., Smith, P., Beer, C., van der Werf,
783 G.R., Gervois, S., Van Oost, K., Tomelleri, E., Freibauer, A., Schulze, E.D.,
784 CARBOEUROPE Synthesis Team, 2010. The European carbon balance. Part 2:
785 croplands. *Global Change Biol.* 16, 1409–1428. doi:10.1111/j.1365-
786 2486.2009.02055.x

787 Coops, N.C., Jassal, R.S., Leuning, R., Black, A.T., Morgenstern, K., 2007.
788 Incorporation of a soil water modifier into MODIS predictions of temperate
789 Douglas-fir gross primary productivity: Initial model development. *Agric. For.*
790 *Meteorol.* 147, 99–109. doi:10.1016/j.agrformet.2007.07.001

791 Falge, E., Baldocchi, D., Olson, R., Anthoni, P., Aubinet, M., Bernhofer, C., Burba, G.,
792 Ceulemans, R., Clement, R., Dolman, H., Granier, A., Gross, P., Grünwald, T.,
793 Hollinger, D., Jensen, N-O., Katul, G., Keronen, P., Kowalski, A., Lai, C.T., Law,
794 B.E., Meyers, T., Moncrieff, J., Moors, E., Munger, J.W., Pilegaard, K., Rannik,
795 Ü., Rebmann, C., Suyker, A., Tenhunen, J., Tu, K., Verma, S., Vesala, T., Wilson,
796 K., Wofsy, S., 2001. Gap filling strategies for defensible annual sums of net
797 ecosystem exchange. *Agric. For. Meteorol.* 107, 43–69. doi:10.1016/S0168-
798 1923(00)00225-2

799 Foley, J.A., Defries, R., Asner, G.P., Barford, C., Bonan, G., Carpenter, S.R., Chapin,
800 F.S., Coe, M.T., Daily, G.C., Gibbs, H.K., Helkowski, J.H., Holloway, T., Howard,
801 E.A., Kucharik, C.J., Monfreda, C., Patz, J.A., Prentice, I.C., Ramankutty, N.,
802 Snyder, P.K., 2005. Global consequences of land use. *Science* 309, 570–574.
803 doi:10.1126/science.1111772

804 Gebremedhin, M.T., Loescher, H.W., Tsegaye, T.D., 2012. Carbon Balance of No-Till
805 Soybean with Winter Wheat Cover Crop in the Southeastern United States. *Agron.*
806 *J.* 104, 1321–1335. doi:10.2134/agronj2012.0072

807 Gebremichael, M., Barros, A., 2006. Evaluation of MODIS Gross Primary Productivity
808 (GPP) in tropical monsoon regions. *Remote Sens. Environ.* 100(2), 150–166.
809 doi:10.1029/2002GB002023

810 Gilmanov, T.G., Verma, S.B., Sims, P.L., Meyers, T.P., Bradford, J.A., Burba, G.G.,
811 Suyker, A.E., (2003). Gross primary production and light response parameters of
812 four Southern Plains ecosystems estimated using long-term CO₂-flux tower
813 measurements. *Global Biogeochem. Cycles* 17, 1071. doi:10.1029/2002GB002023

814 Göckede, M., Foken, T., Aubinet, M., Aurela, M., Banza, J., Bernhofer, C., Bonnefond,
815 J.M., Brunet, Y., Carrara, A., Clement, R., Dellwik, E., Elbers, J., Eugster, W.,
816 Fuhrer, J., Granier, A., Grünwald, T., Heinesch, B., Janssens, I.A., Knohl, A.,
817 Koeble, R., Laurila, T., Longdoz, B., Manca, G., Marek, M., Markkanen, T.,
818 Mateus, J., Matteucci, G., Mauder, M., Migliavacca, M., Minerbi, S., Moncrieff, J.,
819 Montagnani, L., Moors, E., Ourcival, J.-M., Papale, D., Pereira, J., Pilegaard, K.,
820 Pita, G., Rambal, S., Rebmann, C., Rodrigues, A., Rotenberg, E., Sanz, M.J.,
821 Sedlak, P., Seufert, G., Siebicke, L., Soussana, J.F., Valentini, R., Vesala, T.,

822 Verbeeck, H., Yakir, D., (2008). Quality control of CarboEurope flux data – Part 1:
823 Coupling footprint analyses with flux data quality assessment to evaluate sites in
824 forest ecosystems, *Biogeosciences* 5, 433–450. doi:10.5194/bg-5-433-2008

825 Goldewijk, K.K., 2001. Estimating global land use change over the past 300 years: The
826 HYDE Database. *Global Biogeochem. Cycles* 15, 417–433.
827 doi:10.1029/1999GB001232

828 Haszpra, L., Barcza, Z., Bakwin, P.S., Berger, B.W., Davis, K.J., Weidinger, T., 2001.
829 Measuring system for the long-term monitoring of biosphere/atmosphere exchange
830 of carbon dioxide. *J. Geophys. Res.* 106D, 3057–3070. doi:10.1029/2000JD900600

831 Haszpra, L., Barcza, Z., Davis, K.J., Tarczay, K., 2005. Long-term tall tower carbon
832 dioxide flux monitoring over an area of mixed vegetation. *Agric. For. Meteorol.*
833 132, 58–77. doi:10.1016/j.agrformet.2005.07.002

834 Heinsch, F.A., Reeves, M., Votava, P., Kang, S., Milesi, C., Zhao, M., Glassy, J., Jolly,
835 W.M., Loehman, R., Bowker, C.F., Kimball, J.S., Nemani, R.R., Running, S.W.,
836 2003. User’s Guide GPP and NPP (MOD17A2/A3) Products NASA MODIS Land
837 Algorithm. http://datamirror.csdb.cn/modis/resource/doc/MOD17_UsersGuide.pdf

838 Heinsch, F.A., Zhao, M., Running, S.W., Kimball, J.S., Neman, R.R., Davis, K.J.,
839 Bolstad, P.V., Cook, B.D., Desai, A.R., Ricciuto, D.M., Law, B.E., Oechel, W.C.,
840 Kwon, H., Luo, H., Wofsy, S.C., Dunn, A.L., Munger, J.W., Baldocchi, D.D., Xu,
841 L., Hollinger, D.Y., Richardson, A.D., Stoy, P.C., Siqueira, M.B.S., Monson, R.K.,
842 Burns, S.P., Flanagan, L.B., 2006. Evaluation of Remote Sensing Based Terrestrial
843 Productivity From MODIS Using Regional Tower Eddy Flux Network
844 Observations. *IEEE Trans. Geosci. Remote Sens.* 44, 1908–1924.
845 doi:10.1109/TGRS.2005.853936

846 Hidy, D., Barcza, Z., Haszpra, L., Churkina, G., Pintér, K., Nagy, Z., 2011.
847 Development of the Biome-BGC model for simulation of managed herbaceous
848 ecosystems. *Ecol. Modell.* 226, 99–119. doi:10.1016/j.ecolmodel.2011.11.008

849 Horst, T.W., Weil, J.C., 1992. Footprint estimation for scalar flux measurements in the
850 atmospheric surface layer. *Boundary-Layer Meteorol.* 59, 279–296.

851 Huete, A., Justice, C., Leeuwen, W.V., 1999. MODIS vegetation index – MOD13.
852 Algorithm Theoretical Basis Document.
853 http://modis.gsfc.nasa.gov/data/atbd/atbd_mod13.pdf

854 Hwang, T., Kang, S., Kim, J., Kim, Y., Lee, D., Band, L., 2008. Evaluating drought
855 effect on MODIS Gross Primary Production (GPP) with an eco-hydrological
856 model in the mountainous forest, East Asia. *Global Change Biol.* 14, 1–20.
857 doi:10.1111/j.1365-2486.2008.01556.x

858 Janssen, P.H.M., Heuberger, P.S.C., 1995. Calibration of process-oriented models. *Ecol.*
859 *Modell.* 83, 55–66. doi:10.1016/0304-3800(95)00084-9

860 Kanniah, K.D., Beringer, J., Hutley, L.B., Tapper, N.J., Zhu, X., 2009. Evaluation of
861 Collections 4 and 5 of the MODIS Gross Primary Productivity product and
862 algorithm improvement at a tropical savanna site in northern Australia. *Remote*
863 *Sens. Environ.* 113, 1808–1822. doi:10.1016/j.rse.2009.04.013

864 Kim, J., Guo, Q., Baldocchi, D.D., Leclerc, M.Y., Xu, L., Schmid, H.P., 2006.
865 Upscaling fluxes from tower to landscape: Overlaying flux footprints on high-
866 resolution (IKONOS) images of vegetation cover. *Agric. For. Meteorol.* 136, 132-
867 146, <http://dx.doi.org/10.1016/j.agrformet.2004.11.015>

- 868 Kljun, N., Rotach, M.W., Schmid, H.P., 2002. A 3D Backward Lagrangian Footprint
869 Model for a Wide Range of Boundary Layer Stratifications. *Boundary-Layer*
870 *Meteorol.* 103, 205-226.
- 871 Kljun, N., Calanca, P., Rotach, M.W., Schmid, H.P., 2004. A simple parameterisation
872 for flux footprint predictions. *Boundary-Layer Meteorol.* 112, 503–523.
873 doi:10.1023/B:BOUN.0000030653.71031.96
- 874 Knyazikhin, Y., Glassy, J., Privette, J.L., Tian, Y., Lotsch, A., Zhang, Y., Wang, Y.,
875 Morisette, J.T., Votava, P., Myneni, R.B., Nemani, R.R., Running, S.W., 1999.
876 MODIS Leaf Area Index (LAI) and Fraction of Photosynthetically Active
877 Radiation Absorbed by Vegetation (FPAR) Product (MOD15) Algorithm
878 Theoretical Basis Document, <http://eosps.gsfc.nasa.gov/atbd/modistables.html>
- 879 Kutsch, W.L., Aubinet, M., Buchmann, N., Smith, P., Osborne, B., Eugster, W.,
880 Wattenbach, M., Schrumpf, M., Schulze, E.D., Tomelleri, E., Ceschia, E.,
881 Bernhofer, C., Béziat, P., Carrara, A., Di Tommasi, P., Grünwald, T., Jones, M.,
882 Magliulo, V., Marloie, O., Moureaux, C., Olioso, A., Sanz, M.J., Saunders, M.,
883 Sogaard, H., Ziegler, W., 2010. The net biome production of full crop rotations in
884 Europe. *Agric. Ecosyst. Environ.* 139, 336–345. doi:10.1016/j.agee.2010.07.016
- 885 Lasslop, G., Reichstein, M., Papale, D., Richardson, A.D., Arneeth, A., Barr, A., Stoy,
886 P., Wohlfahrt, G., 2010. Separation of net ecosystem exchange into assimilation
887 and respiration using a light response curve approach: critical issues and global
888 evaluation. *Global Change Biol.* 16, 187–208, [http://dx.doi.org/10.1111/j.1365-](http://dx.doi.org/10.1111/j.1365-2486.2009.02041.x)
889 [2486.2009.02041.x](http://dx.doi.org/10.1111/j.1365-2486.2009.02041.x).
- 890 Leuning, R., Cleugh, H.A., Zegelin, S.J., Hughes, D., 2005. Carbon and water fluxes
891 over a temperate Eucalyptus forest and a tropical wet/dry savanna in Australia:
892 measurements and comparison with MODIS remote sensing estimates. *Agric. For.*
893 *Meteorol.* 129, 151–173. doi:10.1016/j.agrformet.2004.12.004
- 894 Lloyd, J., Taylor, J.A., 1994. On the temperature dependence of soil respiration. *Funct.*
895 *Ecol.* 8, 315-323.
- 896 Lobell, D.B., Asner, G.P., 2004. Cropland distributions from temporal unmixing of
897 MODIS data. *Remote Sens. Environ.* 93, 412–422. doi:10.1016/j.rse.2004.08.002
- 898 Ma, S., Churkina, G., Wieland, R., Gessler, A., 2011. Optimization and evaluation of
899 the ANTHRO-BGC model for winter crops in Europe. *Ecol. Modell.* 222, 3662–
900 3679. doi:10.1016/j.ecolmodel.2011.08.025
- 901 McCallum, I., Wagner, W., Schmullius, C., Shvidenko, A., Obersteiner, M., Fritz, S.,
902 Nilsson, S., 2009. Satellite-based terrestrial production efficiency modeling.
903 *Carbon Balance Manage.* 4:8. doi:10.1186/1750-0680-4-8
- 904 Moffat, A.M., Papale, D., Reichstein, M., Hollinger, D.Y., Richardson, A.D., Barr,
905 A.G., Beckstein, C., Braswell, B.H., Churkina, G., Desai, A.R., Falge, E., Gove,
906 J.H., Heimann, M., Hui, D., Jarvis, A.J., Kattge, J., Noormets, A. Stauch, V.J.,
907 2007. Comprehensive comparison of gap-filling techniques for eddy covariance
908 net carbon fluxes. *Agric. For. Meteorol.* 147, 209–232.
909 doi:10.1016/j.agrformet.2007.08.011
- 910 Monteith, J., 1972. Solar radiation and productivity in tropical ecosystems. *J. Appl.*
911 *Ecol.* 9, 747–766.
- 912 Monteith, J., 1977. Climate and efficiency of crop production in Britain. *Philos. Trans.*
913 *R. Soc. London, Ser. B* 281, 277–294.
- 914 Monfreda, C., Ramankutty, N., Foley, J.A., 2008. Farming the planet: 2. Geographic
915 distribution of crop areas, yields, physiological types, and net primary production

- 916 in the year 2000. *Global Biogeochem. Cycles* 22, GB1022
 917 doi:10.1029/2007GB002947.
- 918 Nightingale, J., Coops, N., Waring, R., Hargrove, W., 2007. Comparison of MODIS
 919 gross primary production estimates for forests across the U.S.A. with those
 920 generated by a simple process model, 3-PGS. *Remote Sens. Environ.* 109, 500–
 921 509. doi:10.1016/j.rse.2007.02.004
- 922 Pittman, K., Hansen, M.C., Becker-Reshef, I., Potapov, P.V., Justice, C.O., 2010.
 923 Estimating Global Cropland Extent with Multi-year MODIS Data. *Remote Sensing*
 924 2, 1844–1863. doi:10.3390/rs2071844
- 925 Ramankutty, N., Foley, J.A., 1999. Estimating historical changes in global land cover:
 926 Croplands from 1700 to 1992, *Global Biogeochem. Cycles* 13, 997–1027.
 927 doi:10.1029/1999GB900046
- 928 Ramankutty, N., Foley, J.A., Norman, J., McSweeney, K., 2002. The global distribution
 929 of cultivable lands: Current patterns and sensitivity to possible climate change.
 930 *Global Ecol. Biogeogr.* 11, 377–392. 10.1046/j.1466-822x.2002.00294.x
- 931 Ramankutty, N., Evan, A.T., Monfreda, C., Foley, J.A., 2008. Farming the planet: 1.
 932 Geographic distribution of global agricultural lands in the year 2000. *Global*
 933 *Biogeochem. Cycles* 22, GB1003 doi:10.1029/2007GB002952
- 934 Reich, P.B., Turner, D.P., Bolstad, P., 1999. An approach to spatially distributed
 935 modeling of net primary production (NPP) at the landscape scale and its
 936 application in validation of EOS NPP products. *Remote Sens. Environ.* 70, 69–81.
 937 doi:10.1016/S0034-4257(99)00058-9
- 938 Reichstein, M., Falge, E., Baldocchi, D., Papale, D., Aubinet, M., Berbigier, P.,
 939 Bernhofer, C., Buchmann, N., Gilmanov, T., Granier, A., Grunwald, T.,
 940 Havrankova, K., Ilvesniemi, H., Janous, D., Knohl, A., Laurila, T., Lohila, A.,
 941 Loustau, D., Matteucci, G., Meyers, T., Miglietta, F., Ourcival, J., Pumpan, M.,
 942 2005. On the separation of net ecosystem exchange into assimilation and
 943 ecosystem respiration: review and improved algorithm. *Global Change Biol.* 11,
 944 1424–1439. doi:10.1111/j.1365-2486.2005.001002.x
- 945 Running, S.W., Baldocchi, D.D., Turner, D.P., Gower, S.T., Bakwin, P.S., Hibbard,
 946 K.A., 1999a. A Global Terrestrial Monitoring Network Integrating Tower Fluxes,
 947 Flask Sampling, Ecosystem Modeling and EOS Satellite Data. *Remote Sens.*
 948 *Environ.* 70, 108–127. doi:10.1016/S0034-4257(99)00061-9
- 949 Running, S.W., Nemani, R.R., Glassy, J.M., Thornton, P.E., 1999b. MODIS Daily
 950 Photosynthesis (PSN) and Annual Net Primary Production (NPP) product
 951 (MOD17) algorithm theoretical basis document.
 952 www.ntsg.umd.edu/modis/ATBD/ATBD_MOD17_v21.pdf
- 953 Running, S.W., Nemani, R.R., Heinsch, F.A., Zhao, M., Reeves, M., Hashimoto, H.,
 954 2004. A continuous satellite-derived measure of global terrestrial primary
 955 production. *Bioscience* 54, 547–560. doi:10.1043/0006-
 956 3568(2004)054(0547:ACSMOG)2.0.CO;2
- 957 Schmid, H.P., Lloyd, C.R., 1999. Spatial representativeness and the location bias of flux
 958 footprints over inhomogeneous areas. *Agric. For. Meteorol.* 93, 195-209,
 959 [http://dx.doi.org/10.1016/S0168-1923\(98\)00119-1](http://dx.doi.org/10.1016/S0168-1923(98)00119-1)
- 960 Schulze, E.D., Luyssaert, S., Ciais, P., Freibauer, A., Janssens, I.A., Soussana, J.F.,
 961 Smith, P., Grace, J., Levin, I., Thiruchittampalam, B., Heimann, M., Dolman, A.J.,

962 Valentini, R., Bousquet, P., Peylin, P., Peters, W., Rödenbeck, C., Etiope, G.,
963 Vuichard, N., Wattenbach, M., Nabuurs, G.J., Poussi, Z., Nieschulze, J., Gash, J.H.
964 the CarboEurope Team, 2009. Importance of methane and nitrous oxide for
965 Europe's terrestrial greenhouse-gas balance. *Nature Geoscience* 2, 842–850.
966 doi:10.1038/ngeo686

967 Schwalm, C.R., Williams, C.A., Schaefer, K., Anderson, R., Arain, M.A., Baker, I.,
968 Barr, A., Black, T.A., Chen, G., Chen, J.M., Ciais, P., Davis, K.J., Desai, A.,
969 Dietze, M., Dragoni, D., Fischer, M.L., Flanagan, L.B., Grant, R., Gu, L.,
970 Hollinger, D., Izaurralde, R.C., Kucharik, C., Lafleur, P., Law, B.E., Li, L., Li, Z.,
971 Liu, S., Lokupitiya, E., Luo, Y., Ma, S., Margolis, H., Matamala, R., McCaughey,
972 H., Monson, R.K., Oechel, W.C., Peng, C., Poulter, B., Price, D.T., Riciutto, D.
973 M., Riley, W., Sahoo, A.K., Sprintsin, M., Sun, J., Tian, H., Tonitto, C., Verbeeck,
974 H., Verma, S.B., 2010. A model-data intercomparison of CO₂ exchange across
975 North America: Results from the North American Carbon Program site synthesis.
976 *J. Geophys. Res.* 115, G00H05, doi:10.1029/2009JG001229.

977 Sims, D.A., Rahman, A.F., Cordova, V.D., Baldocchi, D.D., Dennis, Flanagan, L.B.,
978 Goldstein, A.H., Hollinger, D.Y., Misson, L., Monson, R.K., Schmid, H.P., Wofsy,
979 S.C., Xu, L., 2005. Midday values of gross CO₂ flux and light use efficiency
980 during satellite overpasses can be used to directly estimate eight-day mean flux.
981 *Agric. For. Meteorol.* 131, 1–12. doi:10.1016/j.agrformet.2005.04.006

982 Stoy, P.C., Katul, G.G., Siqueira, M.B.S. Juang, J.-Y., Novick, K.A., Uebelherr, J.M.,
983 Oren, R., 2006. An evaluation of models for partitioning eddy covariance-
984 measured net ecosystem exchange into photosynthesis and respiration. *Agric. For.*
985 *Meteorol.* 141, 2–18. doi:10.1016/j.agrformet.2006.09.001

986 Strahler, A., Muchoney, D., Borak, J., Friedl, M., Gopal, S., Lambin, E., Moody, A.,
987 1999. MODIS Land cover product Algorithm Theoretical Basis Document
988 (ATBD). http://modis.gsfc.nasa.gov/data/atbd/atbd_mod12.pdf

989 Suyker, A.E., Verma, S.B., Burba, G.G., Arkebauer, T.J., 2005. Gross primary
990 production and ecosystem respiration of irrigated maize and irrigated soybean
991 during a growing season. *Agric. For. Meteorol.* 131, 180–190.
992 doi:10.1016/j.agrformet.2005.05.007

993 Thornton, P.E., Hasenauer, H., White, M.A., 2000. Simultaneous estimation of daily
994 solar radiation and humidity from observed temperature and precipitation:
995 application over complex terrain in Austria. *Agric. For. Meteorol.* 104, 255–271.
996 doi:10.1016/S0168-1923(00)00170-2

997 Turner, D.P., Ritts, W.D., Cohen, W.B., Maeirsperger, T.K., Gower, S.T., Kirschbaum,
998 A.A., Running, S.W., Zhao, M., Wofsy, S.C., Dunn, A.L., Law, B.E., Campbell,
999 J.L., Oechel, W.C., Kwon, H.J., Meyers, T.P., Small, E.E., Kurc, S.A., Gamon,
1000 J.A., 2005. Site-level evaluation of satellite-based global terrestrial gross primary
1001 production and net primary production monitoring. *Global Change Biol.* 11(4),
1002 666–684. doi:10.1111/j.1365-2486.2005.00936.x

1003 Turner, D.P., Ritts, W.D., Cohen, W.B., Gower, S.T., Running, S.W., Zhao, M., Costa,
1004 M.H., Kirschbaum, A.A., Ham, J.M., Saleska, S.R., Ahl, D.E., 2006. Evaluation of
1005 MODIS NPP and GPP products across multiple biomes. *Remote Sens. Environ.*
1006 102, 282–292. doi:10.1016/j.rse.2006.02.017

1007 Turner, D.P., Ollinger, S.V., Kimball J.S., 2004. Integrating remote sensing and
1008 ecosystem process models for landscape- to regional-scale analysis of the carbon

1009 cycle. *BioScience* 54, 573–584. doi:10.1641/0006-
 1010 3568(2004)054[0573:IRSAEP]2.0.CO;2
 1011 Van Oijen, M., Rougier, J., Smith, R., 2005. Bayesian calibration of process-based
 1012 forest models: bridging the gap between models and data. *Tree Physiol.* 25, 915–
 1013 927. doi:10.1093/treephys/25.7.915
 1014 Vetter, M., Churkina, G., Jung, M., Reichstein, M., Zaehle, S., Bondeau, A., Chen, Y.,
 1015 Ciais, P., Feser, F., Freibauer, A., Geyer, R., Jones, C., Papale, D., Tenhunen, J.,
 1016 Tomelleri, E., Trusilova, K., Viovy, N., Heimann, M., 2008. Analyzing the causes
 1017 and spatial pattern of the European 2003 carbon flux anomaly using seven models.
 1018 *Biogeosciences* 5, 561–583. doi:10.5194/bg-5-561-2008
 1019 Wang, W., Davis, K.J., Cook, B.D., Butler, M.P., Ricciuto, D.M., 2006. Decomposing
 1020 CO₂ fluxes measured over a mixed ecosystem at a tall tower and extending to a
 1021 region: A case study. *J. Geophys. Res.* 111, G02005. doi:10.1029/2005JG000093
 1022 Wang, W., Dungan, J., Hashimoto, H., Michaelis, A.R., Milesi, C., Ichii, K., Nemani,
 1023 R.R., 2011. Diagnosing and assessing uncertainties of terrestrial ecosystem models
 1024 in a multimodel ensemble experiment: 1. Primary production. *Global Change Biol.*
 1025 17, 1350–1366. doi:10.1111/j.1365-2486.2010.02309.x
 1026 Wattenbach, M., Sus, O., Vuichard, N., Lehuger, S., Gottschalk, P., Li, L., Leip, A.,
 1027 Williams, M., Tomelleri, E., Kutsch, W.L., Buchmann, N., Eugster, W., Dietiker,
 1028 D., Aubinet, M., Ceschia, E., Béziat, P., Grünwald, T., Hastings, A., Osborne, B.,
 1029 Ciais, P., Cellier, P., Smith, P., 2010. The carbon balance of European croplands:
 1030 A cross-site comparison of simulation models. *Agric. Ecosyst. Environ.* 139, 419–
 1031 453. doi:10.1016/j.agee.2010.08.004
 1032 Yang, F., Ichii, K., White, M.A., Hashimoto, H., Michaelis, A.R., Votava, P., Zhu, A.-
 1033 X., Huete, A., Running S.W., Nemani, R.R., 2007. Developing a continental-scale
 1034 measure of gross primary production by combining MODIS and AmeriFlux data
 1035 through Support Vector Machine approach. *Remote Sens. Environ.* 110(1), 109–
 1036 122. doi:10.1016/j.rse.2007.02.016
 1037 Zhang, Y., Yu, Q., Jiang, J., Tang, Y., 2008. Calibration of Terra/MODIS gross primary
 1038 production over an irrigated cropland on the North China Plain and an alpine
 1039 meadow on the Tibetan Plateau. *Global Change Biol.* 14, 757–767.
 1040 doi:10.1111/j.1365-2486.2008.01538.x
 1041 Zhao, M., Heinsch, F.A., Nemani, R.R., Running, S.W., 2005. Improvements of the
 1042 MODIS terrestrial gross and net primary production global data set. *Remote Sens.*
 1043 *Environ.* 95, 164–176. doi:10.1016/j.rse.2004.12.011
 1044 Zhao, M., Running, S.W., Nemani, R.R., 2006. Sensitivity of Moderate Resolution
 1045 Imaging Spectroradiometer (MODIS) terrestrial primary production to the
 1046 accuracy of meteorological reanalyses. *J. Geophys. Res.* 111, G01002.
 1047 doi:10.1029/2004JG000004
 1048

1049 Table 1. Climate data for the Hegyhátsál region. Annual sums of photosynthetically
 1050 active photon flux density (PPFD) and average daytime vapor pressure deficit (VPD)
 1051 are measured locally at Hegyhátsál. 2001–2006 air temperature and precipitation data
 1052 are from the nearby (~17 km) Rábagyarmat climate station, while the 1981-2010 means
 1053 are from Farkasfa regional meteorological observatory (~26 km from tower). A
 1054 comparison of measured and GMAO-based VPD is also shown. Vegetation period
 1055 denotes the period from beginning of March to end of October.
 1056
 1057

		1981-2010	2001	2002	2003	2004	2005	2006
average temperature (°C)	vegetation period	13.8	15.4	15.1	15.3	13.9	14.1	14.8
	whole year	9.5	10.7	11.3	10.6	9.8	9.6	10.3
cumulative precipitation (mm)	vegetation period	588	466	469	381	564	595	604
	whole year	762	550	598	487	705	801	738
sum of PPFD (mol m ⁻²)	vegetation period	n.a.	7611	7359	8020	7086	7540	7261
	whole year	n.a.	8530	8120	9047	7931	8494	8258
average daytime VPD (kPa)	vegetation period	n.a.	0.761	0.801	1.045	0.664	0.704	0.670
	whole year	n.a.	0.510	0.608	0.774	0.521	0.541	0.451
GMAO VPD versus observation	RMSE (Pa)	-	282	264	301	397	376	277
	Bias (Pa)	-	109	65	134	213	187	105
	R ²	-	0.791	0.784	0.884	0.747	0.724	0.767

1058

1059 Table 2. Overview of the properties of different model setups used in this study.

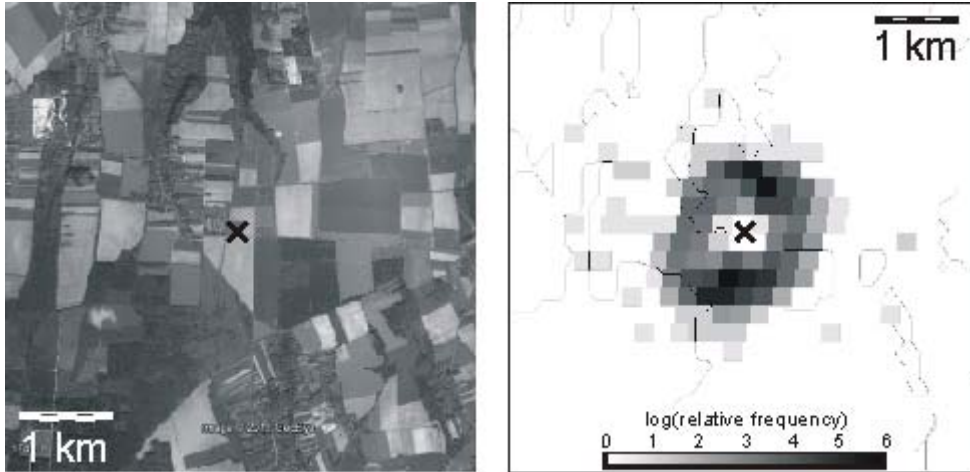
abbreviation	input data			spatial resolution	utilization of footprint model
	meteorology input	FPAR	land cover		
GPP-GMAO	GMAO	MOD15	MOD12	1 km	no
GPP-met	local meteorology	MOD15	MOD12	1 km	no
GPP-FP	local meteorology	MOD15	MOD12	1 km	yes
GPP-NDVI	local meteorology	linear dependence on NDVI	CORINE-2000	250 m	yes

1060

1061 Table 3. Indicators of model performance (cf. Sections 2.4 and 2.5). Note that GPP–
 1062 NDVI is not available before 2003 (launch of Aqua satellite in May 2002). The best
 1063 values of the indicators are highlighted in bold font
 1064
 1065

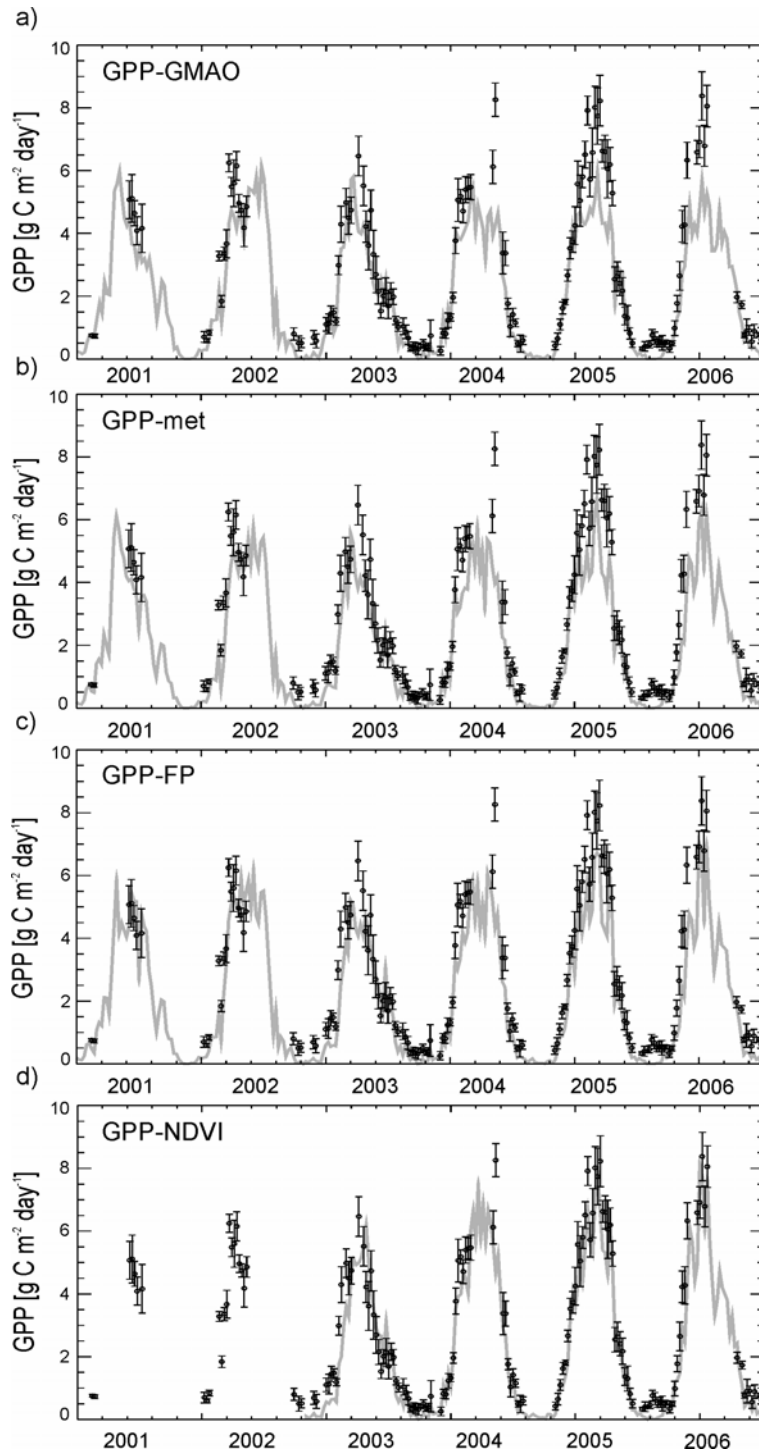
	period	RMSE	IA	ME	KR	R ²	BIAS
GPP-GMAO	2001-2006	1.095	0.930	0.783	0.812	0.905	-0.680
	2003-2006	1.128	0.927	0.778	0.817	0.902	-0.672
GPP-met	2001-2006	1.134	0.928	0.767	0.805	0.911	-0.801
	2003-2006	1.163	0.926	0.764	0.818	0.916	-0.810
GPP-FP	2001-2006	0.999	0.949	0.819	0.795	0.895	-0.634
	2003-2006	1.031	0.946	0.815	0.816	0.915	-0.703
GPP-NDVI	2003-2006	0.815	0.969	0.884	0.823	0.917	-0.426

1066

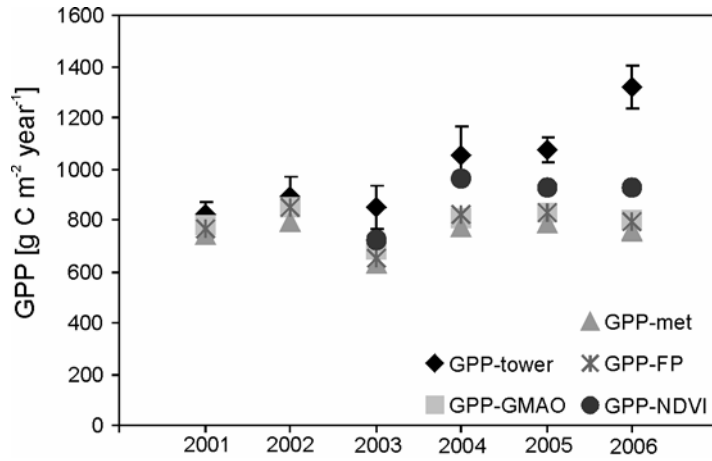


1067
 1068
 1069
 1070
 1071
 1072
 1073
 1074
 1075

Figure 1. a) Satellite image of the Hegyhátsál region (source: Google Earth). b) Footprint climatology of the tall tower for 2007 (representative for all selected years). Footprint climatology is visualized by the relative frequency of the contribution of the different, discretized land cover elements using the 250 m x 250 m resolution of the MODIS NDVI grid. X symbol marks the location of the flux tower. Contour lines show the land cover elements defined by the CORINE2000 database.

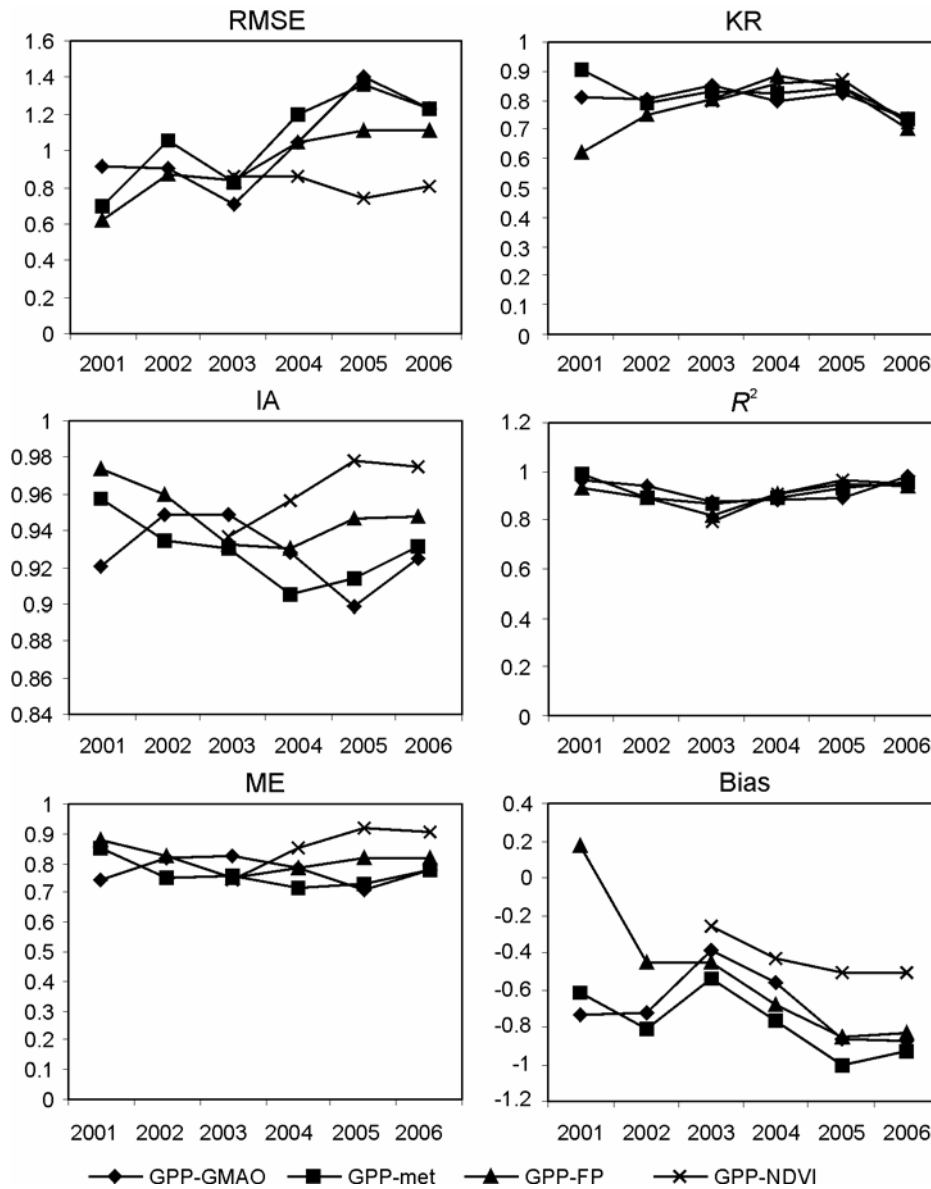


1076
 1077 Figure 2. GPP based on EC measurements (GPP-tower; circles) and simulations (solid
 1078 line): a) GPP-GMAO, b) GPP-met, c) GPP-FP and d) GPP-NDVI for the period of
 1079 2001-2006. See Section 2.4. for definitions. Uncertainty of GPP-tower is also shown
 1080 (one uncertainty range is plotted as error bar).



1081
 1082
 1083
 1084
 1085
 1086

Figure 3. Annual sums of GPP based on EC tower measurements and model calculations. Uncertainties for tower based GPP are also shown (calculated as half of the difference between the daily maximum and minimum GPP estimate). See 2.4 for model description. Note that GPP-tower in 2006 may be biased due to a large data gap.



1087
 1088
 1089
 1090
 1091

Figure 4. Yearly indicators of model performance for different model runs. Note that GPP-NDVI was not available on an annual basis before 2003 (launch of Aqua satellite in May 2002).